JOURNAL OF MATERIALS SCIENCE 24 (1989) 3878–3887

Crystal defects and coherent intergrowth of α- and β-crystals in Y–Ce doped sialon materials

PER-OLOF OLSSON
Department of Inorganic Chemistry, Arrhenius Laboratory, University of Stockholm, S-106 91 Stockholm, Sweden

Sialon material doped with a mixture of yttrium and cerium in a molar ratio of 1 to 3, up to a total amount of 6 wt% has been investigated with high resolution transmission electron microscopy (HREM). The α-sialon crystals were shown to contain defects of types not previously reported. These include stacking faults, shear and coherent intergrowth of α- and β-sialon crystals. For some of the defects structural models are proposed and verified by image simulations.

1. Introduction

Polyphase sialon ceramics have received considerable attention in recent years due to their good physical and chemical properties. These properties depend strongly on the phases present at the grain boundaries and on the structural defects in the individual sialon grains, which makes the control of these features essential. A powerful method for studying these factors is high-resolution transmission electron microscopy (HREM). Such investigations have been published by various groups. Hiraga [1] and Knowles [2] showed images of the unfaulted structure and Hiraga also showed examples of point defects. The problem of crack propagation in silicon nitride crystals was studied by Kakibayashi *et al.* [3]. They also showed examples of line faults found in the interior of sialon crystals. Sasaki *et al.* [4] gave an example of the determination of the displacement vector for planar defects found in silicon nitride. Besides these high-resolution studies, a number of articles have been published concerning the microstructure of silicon nitride-based materials where various defects have been found. Among these, Chatfield *et al.* [5] performed a microstructural investigation of α–β yttrium sialon materials. They found that in some crystals dislocations could be seen which originated in compositional variations in the crystals. Various faults in the structure of sialon materials have also been seen by other groups [6–8]. The conclusion to be drawn from these articles is that a relatively high frequency of defects can be expected in these materials.

The present study forms a part of a larger project where possible replacements for Y_2O_3 as a sintering aid are investigated. This is of commercial interest due to the high cost of Y_2O_3. A preliminary report concerning the (Y, Nd)-sialon system has recently been prepared [9]. The present paper deals with the possibility of using CeO_2 in combination with Y_2O_3.

The interest in the use of CeO_2 as sintering aid for silicon nitride [10–12] or for sialon material [13] has been rather limited. This is probably due to the mixed valence problem of cerium which can be both tri- and tetravalent. However, the published results indicate that the Ce–Si–Al–O–N system resembles the corresponding yttria system, implying for instance that an α-sialon phase containing cerium is formed. Mah *et al.* [12] have proposed a sintering mechanism for silicon nitride doped with CeO_2 which involves the formation of cerium silicates during the sintering process. These intermediate phases are said to stabilize the trivalent state of cerium.

The present study shows some examples of defects found in α-sialon grains, and structural models for these are given. In addition to this, coherent intergrowth of α- and β-sialon crystals without any detectable intergranular phase is demonstrated and discussed.

2. The crystal structure

The structures of the two existing modifications of sialon; α and β, can be derived from the corresponding structures of silicon nitride [14, 15] by partly replacing silicon by aluminium and nitrogen oxygen [16, 17]. This means that the crystal structures of α- and β-sialon can be described as stackings of Si–Al–O–N layers in either an ABAB . . . sequence (β) or an ABCD . . . sequence (α) (Fig. 1). Note that the CD layers are related to the AB layers by a 180° rotation. This gives rise to continuous tunnels in β and closed interstices in α. In the case of α (space group $P31c$), the general formula is $M_x(Si, Al)_{12}(O, N)_{16}$, $x \leqslant 2$, where M = Li, Be, Mg, Ca, Sc, Y or Ln have been reported. The general formula for β-sialon (space group $P6_3/m$) is $Si_{6-z}Al_zO_zN_{8-z}$, with z ranging from 0 to about 4 depending on the preparation method used. The unit cell parameters follow a linear dependence of the z-value, $a = 7.603(6) + z.\ 0.0296(4)$ and $c = 2.907(8) + z.\ 0.0255(6)$ [18].

3. Experimental procedure

A detailed description of the synthesis is given by Ekström *et al.* [18], and thus only a brief outline will be given here. The initial powder mixture consisted of 80 wt% Si_3N_4 (HC Starck-Berlin, LC1), 8 wt% Al_2O_3 (ALCOA A16SG), 6 wt% AlN (HC Starck-Berlin,

0022–2461/89 $03.00 + .12

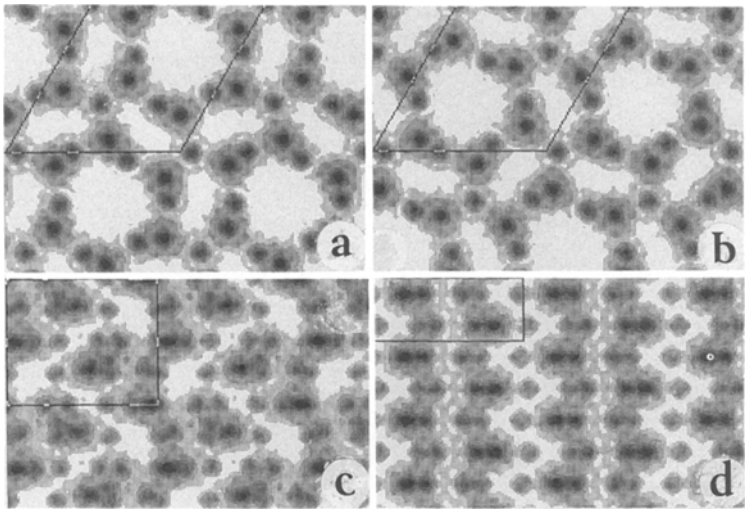

Figure 1 (a) Bounded projection ($\frac{1}{2}c$) along the c axis of the α-sialon structure, comprising the A and B layers of tetrahedra. (b) The same for the other half of the cell, with the C and D layers. (c) The total [1 0 0] projection of α-sialon, the c axis vertical. (d) Corresponding projection of the β-sialon structure.

Grade A) and 6 wt % sintering aid. The latter was a mixture of Y_2O_3 (HC Starck-Berlin > 99.9%) and CeO_2 (H C Starck-Berlin, Chemical Grade) giving a mole ratio of cerium to yttrium equal to 3. After milling, the powder was pressed at 125 MPa to pellets of the size 16 × 16 × 6 mm^3 and sintered at 1775° C in nitrogen for 2 h. For the TEM studies a plate less than 0.2 mm thick was cut from one sample with a wire saw. The final thinning was made by argon-ion milling. To prevent charging in the microscope the specimen was covered with an amorphous carbon layer. The TEM investigations were made in a JEOL 200CX microscope equipped with a top entry goniometer stage with a possible tilt of + − 10° about two axes. The point-to-point resolution of the microscope is about 0.25 nm. Energy dispersive X-ray analysis was made in a JEOL-880 scanning microscope equipped with a LINK AN 10000 EDS analyser.

Image calculations according to the multislice method were performed with a locally modified version of the SHRLI-program package [19]. The atomic coordinates given by Izumi *et al.* [16] for α and Van Dijen *et al.* [17] for β were used. Due to lack of published structural data for the cerium containing α-sialon phase, we have used the structure of Y-α-sialon and partially replaced the yttrium atoms by cerium atoms. For defect structures the periodic continuation approximation was used [20, 21]. A Kontron–IPS system was used for image processing. Phase analysis was made with the use of X-ray powder patterns recorded in a Gunier-Hägg focusing camera (Cu $K_{\alpha 1}$ radiation, silicon as internal standard with a = 5.430 88) [22].

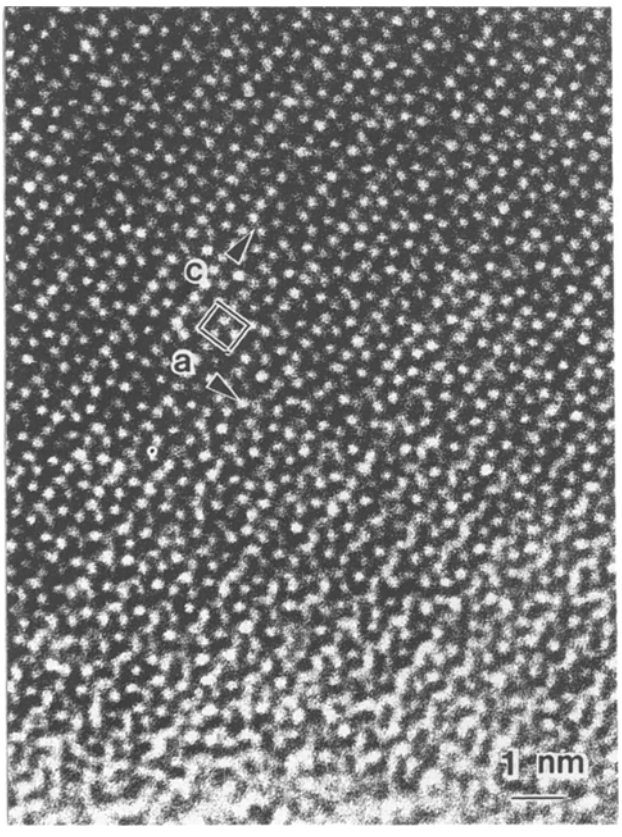

Figure 2 An [1 0 0] image of an Y-α-sialon crystal, showing the normal symmetry in accordance with the space group $P31c$ (Fig. 1c).

4. Analysis

The X-ray analysis showed that the sample contained

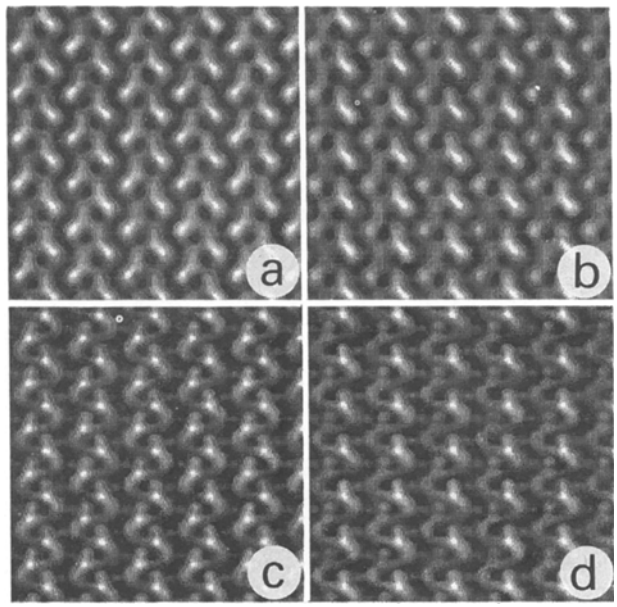

Figure 3 Calculated images along [1 0 0] for the Y-α structure (a, c) [16] and for the hypothetical Ce-Y-α structure (b, d). In the latter case, different occupancy factors have been used for the two cation sites namely 0.42 for cerium at one site and 0.12 for yttrium at the other. The loss of vertical symmetry in (b) and (d) is apparent. The images are calculated for a defocus of − 52.2 nm and a thickness of 3.9 nm (a, b) and 11.7 nm (c, d).

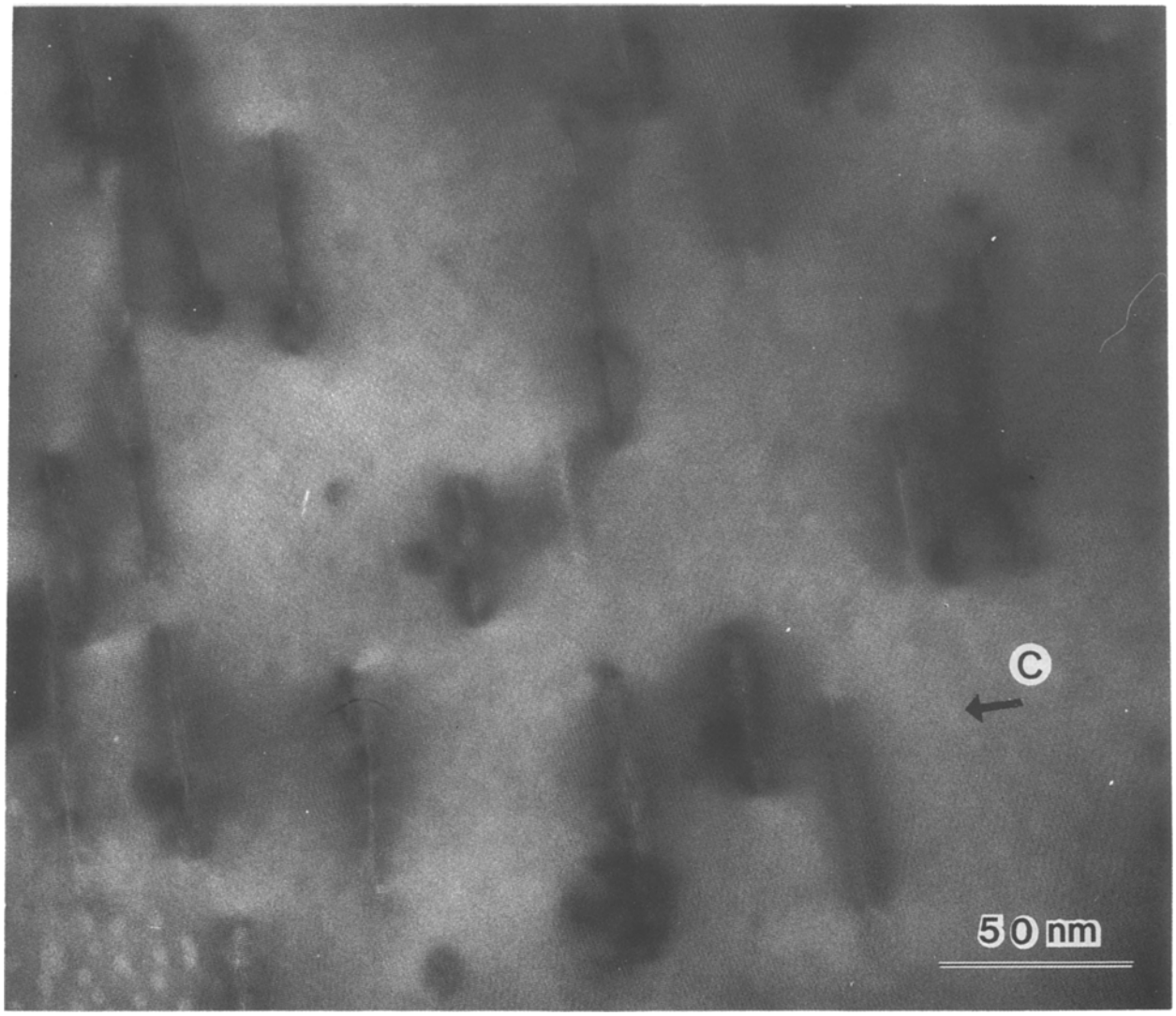

Figure 4 An [1 0 0] image of α-sialon showing typical faults perpendicular to the *c* axis. The direction of the *c* axis is shown by an arrow.

a mixture of α- and β-sialon phases and crystalline intergranular phases. The cell parameters obtained for the α-phase were $a = 0.7797(3)$ nm and $c = 0.5678(2)$ nm and for the β-phase $a = 0.76203(7)$ nm and $c = 0.29190(3)$ nm. The values for the β-phase correspond to a z value of about 0.5 [18]. For determining the ratio of α to β, a simple method based on the uncorrected intensities of the (102) and (210) reflections of the α-phase and the (101) and (210) lines of the β-phase was used. This gave the result that about 84% of the sialon crystals were of the β-type. Two weak unindexed reflections indicated that small amounts of intergranular phases were also present in addition to the sialon phases. With the use of electron diffraction one of these was identified as the 12*H* Si–Al–O–N polytype. The TEM studies also revealed the occurrence of glassy pockets and thin films between most grains. An EDS microanalysis of the α-sialon crystals showed that these contained about 2 at % Ce. This corresponds to an x-value of about 0.5. No cerium could be detected in the β-sialon grains, and yttrium was found neither in the α- nor in the β-sialon crystals. It has to be pointed out, however, that small quantities of yttrium (< 1 at %) might be present in the α-sialon particles without being detected, due to partial overlap of the Si*K* (1.740 eV) line and the Y*L* (1.992 eV) line. When examining the glassy pockets we found them to contain both yttrium and cerium in relatively large amounts.

5. Electron microscopy

A typical HREM image of an Y-α-sialon crystal (without cerium) along [100] is shown in Fig. 2. The glide plane associated with the space group *P*31*c* (Fig. 1c) is clearly visible. Calculated images based on this structure is shown in Figs 3a and c. However, the HREM investigation of the sample showed that the [100] projection of α-sialon had lower symmetry than given by the Y-α-sialon structure model. The glide plane parallel to the *c* axis was not found in the experimental images (see below). This could be an artifact due to either crystal or beam tilt. However, since the same asymmetry was observed in all the α-sialon crystals examined along the [100] projection, randomly orientated around this axis, it was interpreted as a structural feature. A cause of this asymmetry may be different site preferences of the cerium and yttrium atoms in the α-sialon structure. In the Y-α-sialon structure the two sites (1/3, 2/3, 0.242) and (2/3, 1/3, 0.742) are available for yttrium and cerium. Tentative calculations were made assuming an occupancy of 0.42 for cerium at one site and 0.12 for yttrium at the

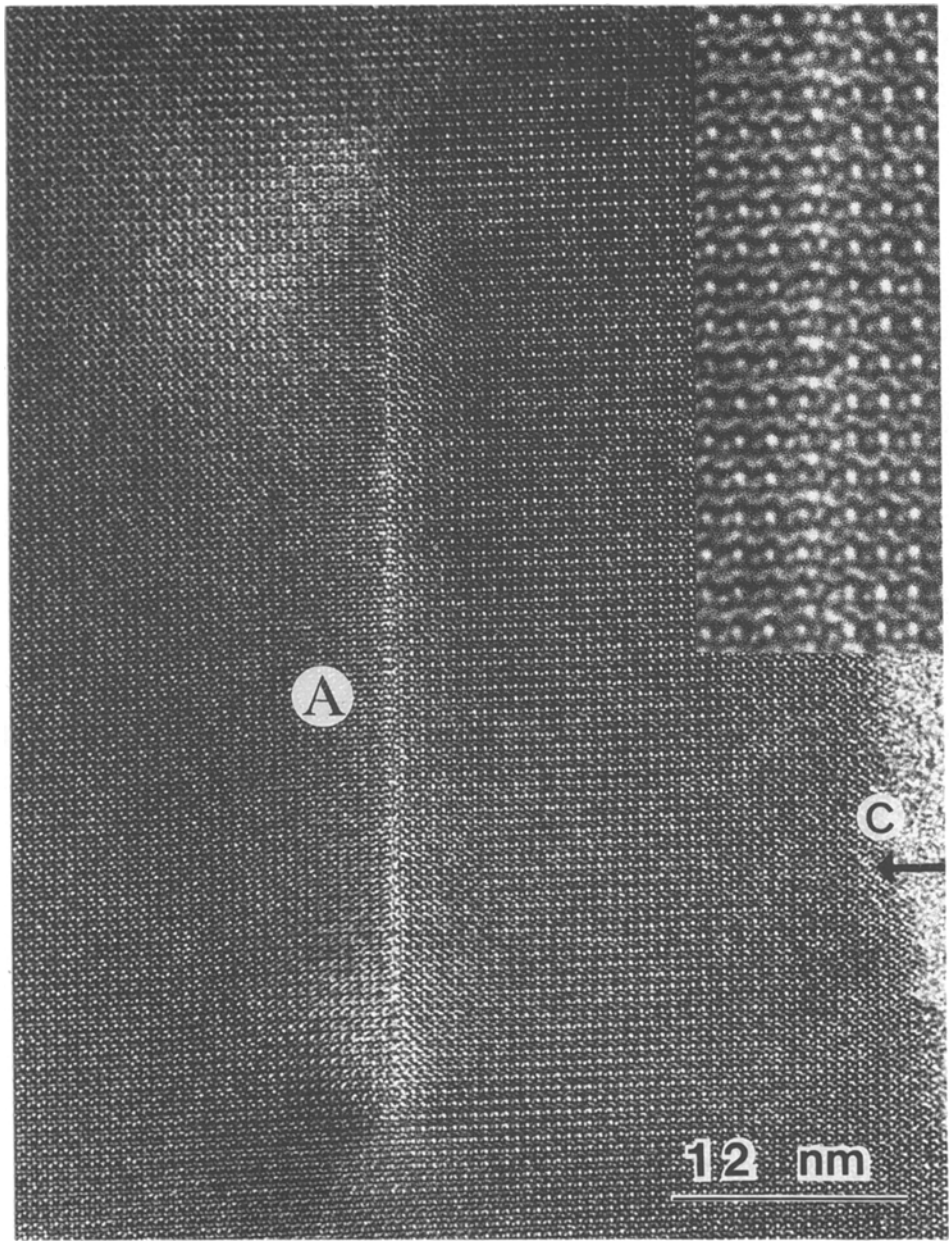

Figure 5 A [1 0 0] image of an α-sialon with a defect perpendicular to the *c* axis (shown by an arrow). The insert shows the part labelled A at higher magnification.

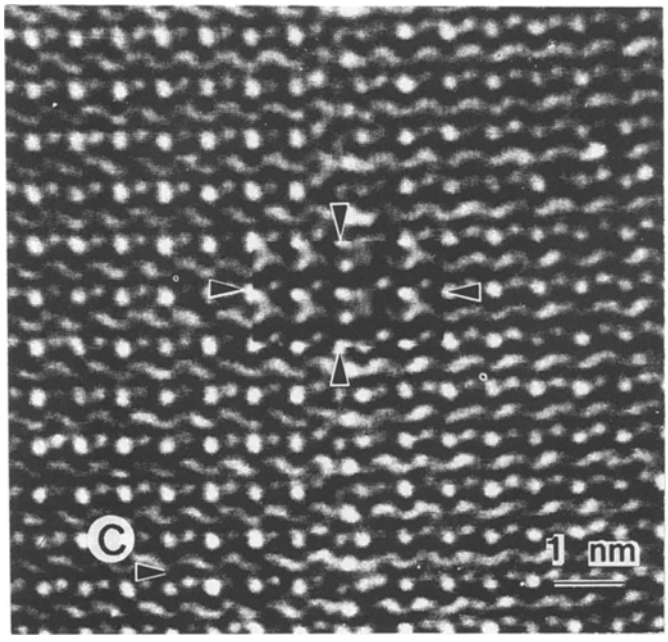

Figure 6 Magnified area of Fig. 5 across the defect near A, with an inserted calculated image indicated by arrows. The image was calculated for a thickness of 15 nm and a defocus of −87.2 nm.

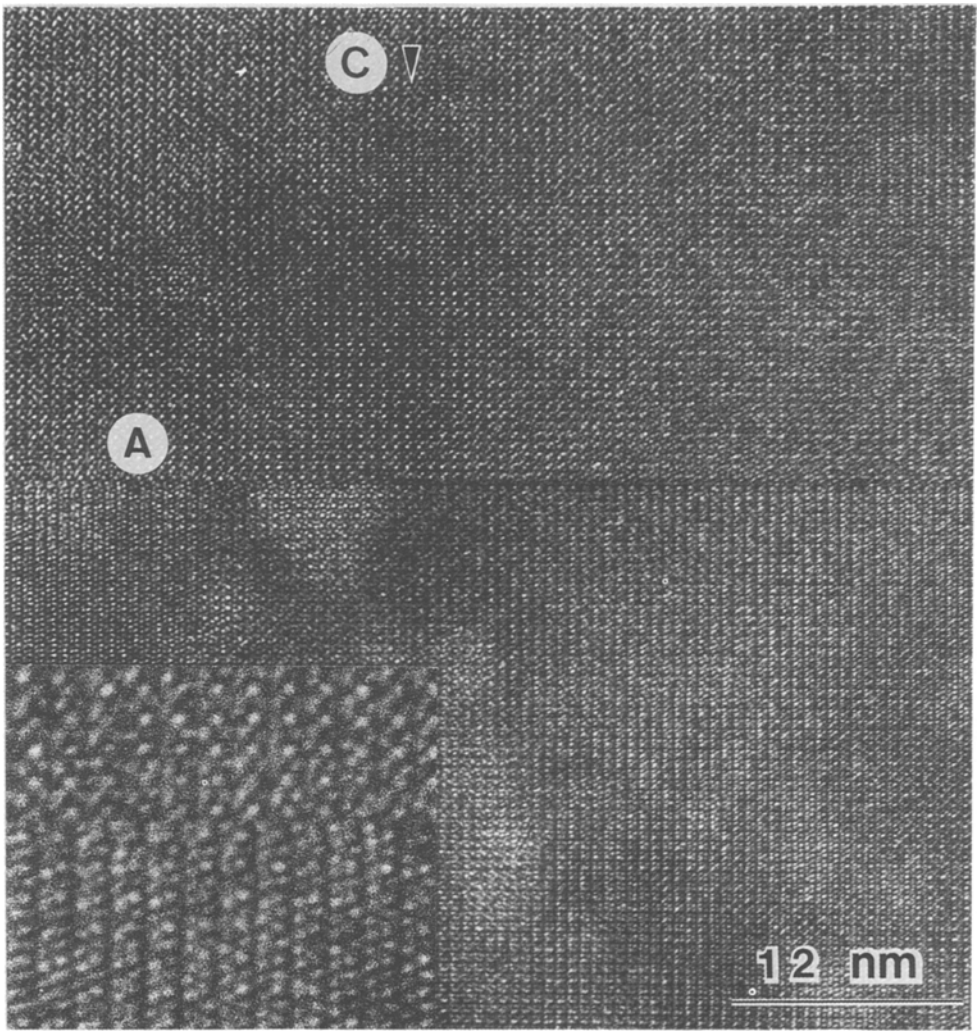

Figure 7 [1 0 0] image of α-sialon, showing a boundary with a translation of the lattice along the *a* axis. The insert shows part of the defect labelled A.

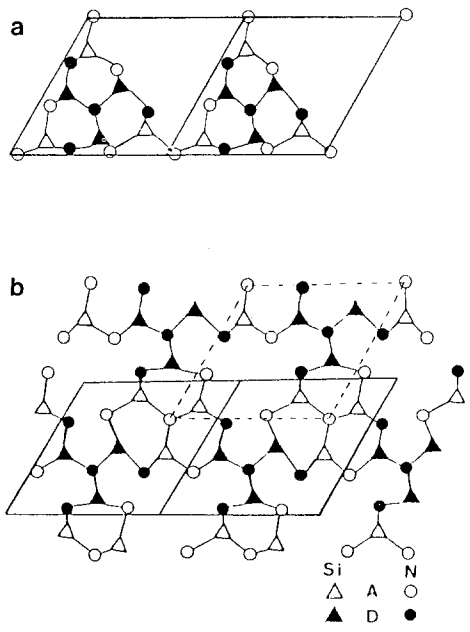

Figure 8 [0 0 1] structural model showing the possibility of connecting the normal structure (a) with a lattice translated $\frac{1}{3}a + \frac{2}{3}b$. The normal structure is seen in a, (the B and C layers occupy the upper right-hand part of the unit cell at other levels) and the sheared lattice is shown in b. The solid unit cells are related to the full symbols (D-layer), whereas the dashed line is associated with the open symbols (A-layer).

other. The simulated images display the required asymmetry i.e. the glide plane parallel to the *c* axis is absent. Examples of calculated images of the proposed Ce-Y-α-sialon structure are shown in Figs 3b and d. There is a possibility that the occupancy at the two cation sites may vary within the same crystal as a consequence of local concentration gradients. This is especially likely in the defect zones. This is probably the reason why it is sometimes difficult to obtain a perfect match between calculated and experimental image. The different occupancy at the two positions is also likely to perturb the Si–Al–O–N network slightly. For the different structure models discussed below, the asymmetrical Ce-Y-α-sialon model is used.

Fig. 4 shows an α-sialon crystal at somewhat lower magnification viewed along the *a* axis. Numerous defects are seen, orthogonal to the *c* axis. Due to strain in the lattice, dark contrast zones are visible around the defects. The defects appear to be two dimensional, with extensions essentially perpendicular to the *c* axis. This type of defect is fairly common in the α-sialon crystals found in the investigated sample but has not been observed by us in materials containing only Y_2O_3 as sintering aid. One defect of this type is shown at larger magnification in Fig. 5. In the central part of the

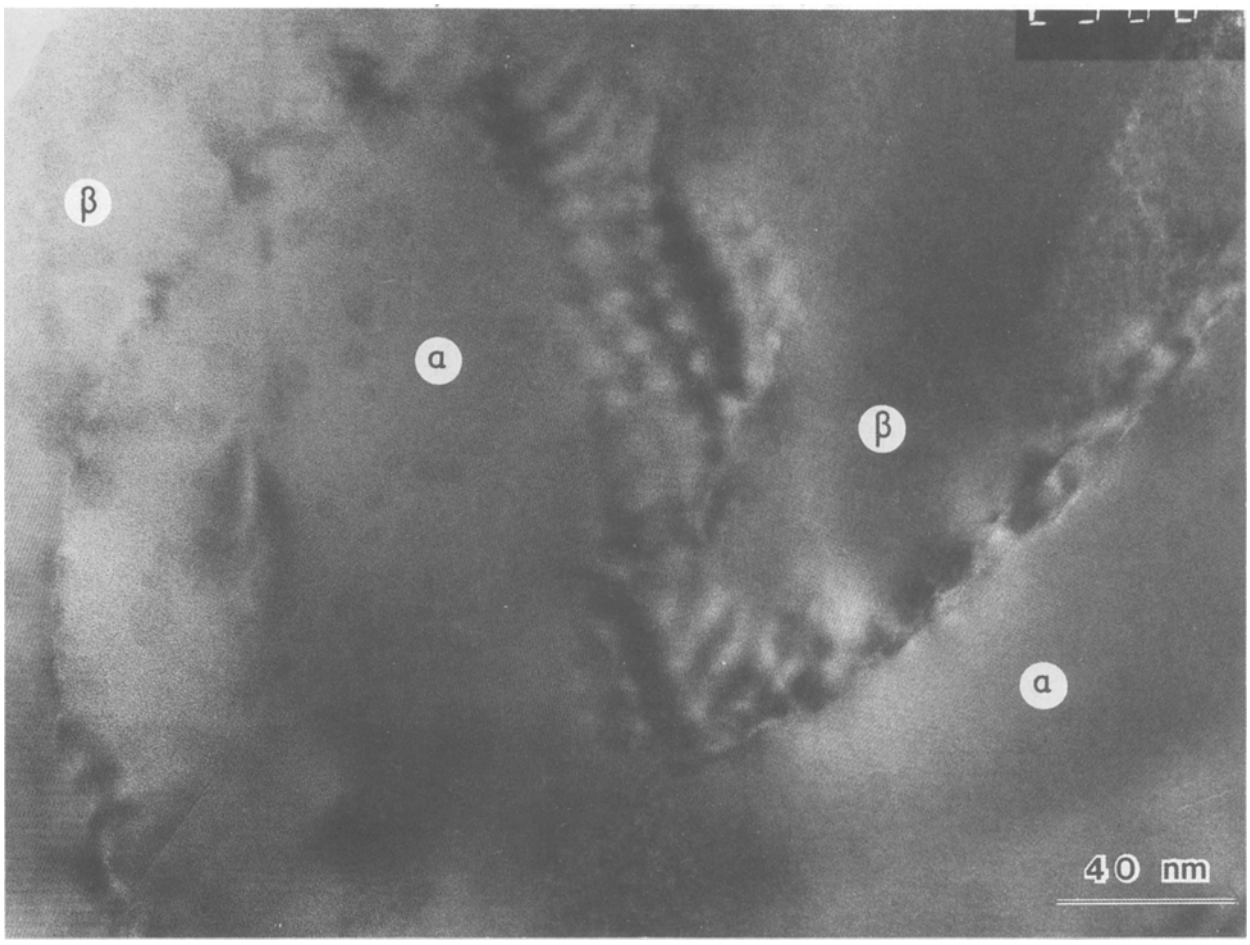

Figure 9 Image of α to β intergrowth. The transformation zone is seen to form a warped pattern in the crystal dividing it into α- and β-structure parts.

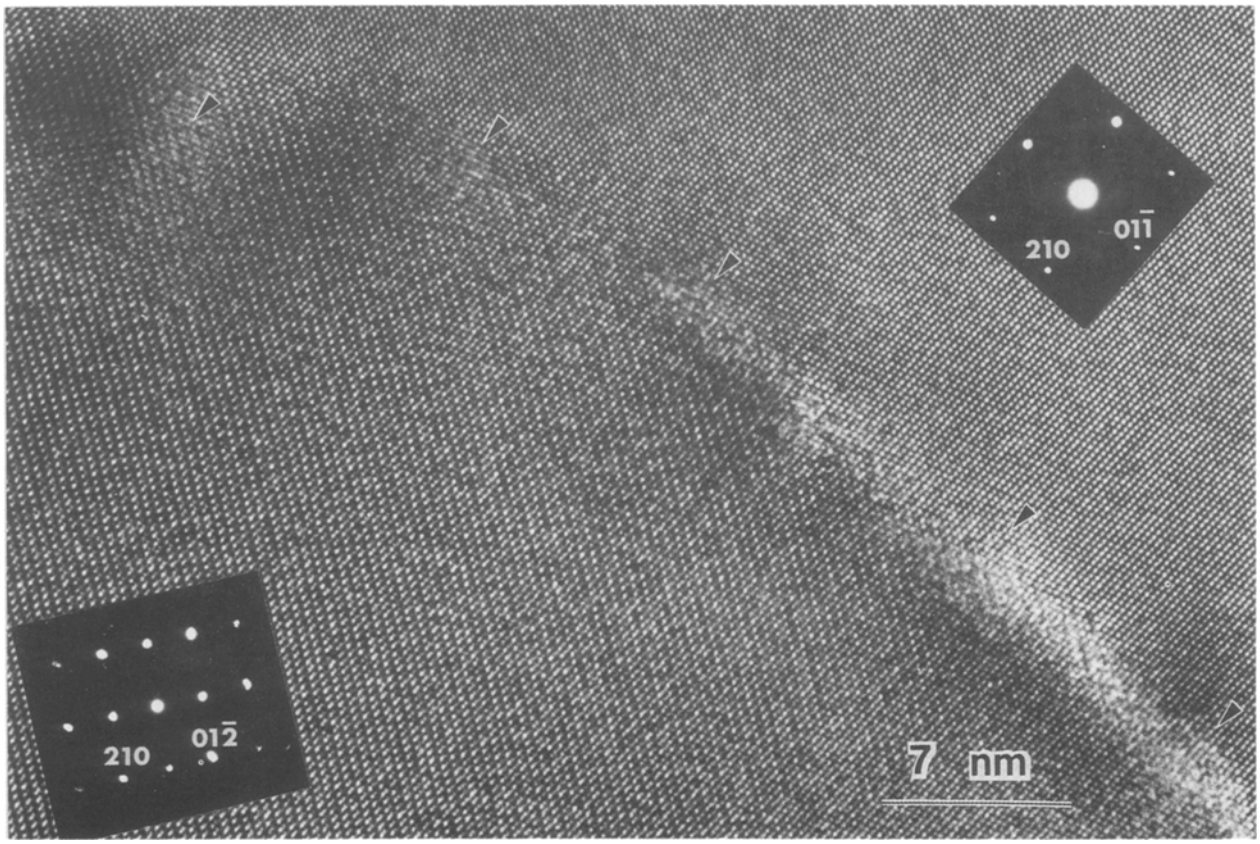

Figure 10 Image of coherent intergrowth from α (viewed along $\bar{1}21$) to β (viewed along $\bar{1}22$). The disordered areas containing edge dislocations are indicated by pointers. The image shows the same crystal as in Fig. 9.

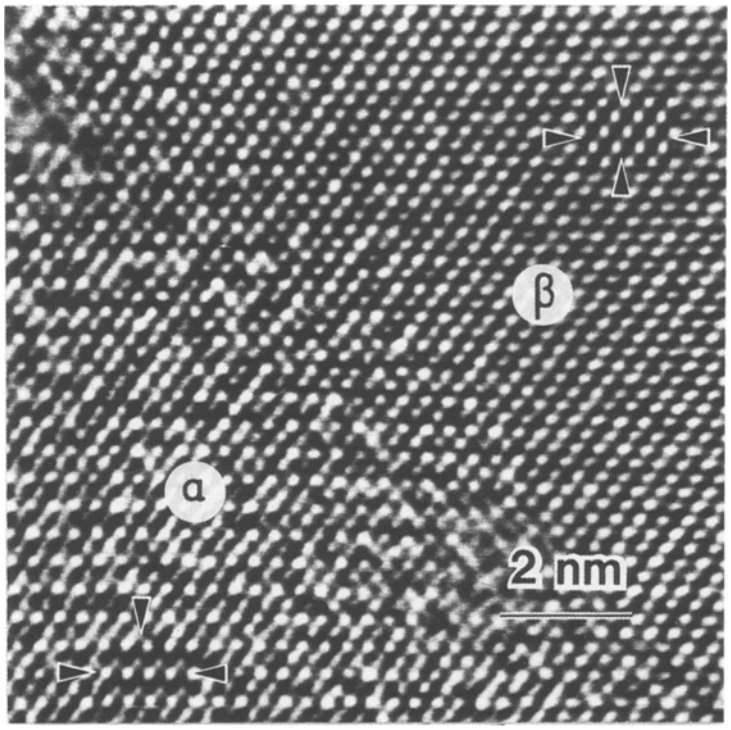

Figure 11 Magnified area of Fig. 10 with inserted calculated images for a thickness of 8 nm and a defocus of −52.2 nm. The calculated images are indicated by arrows.

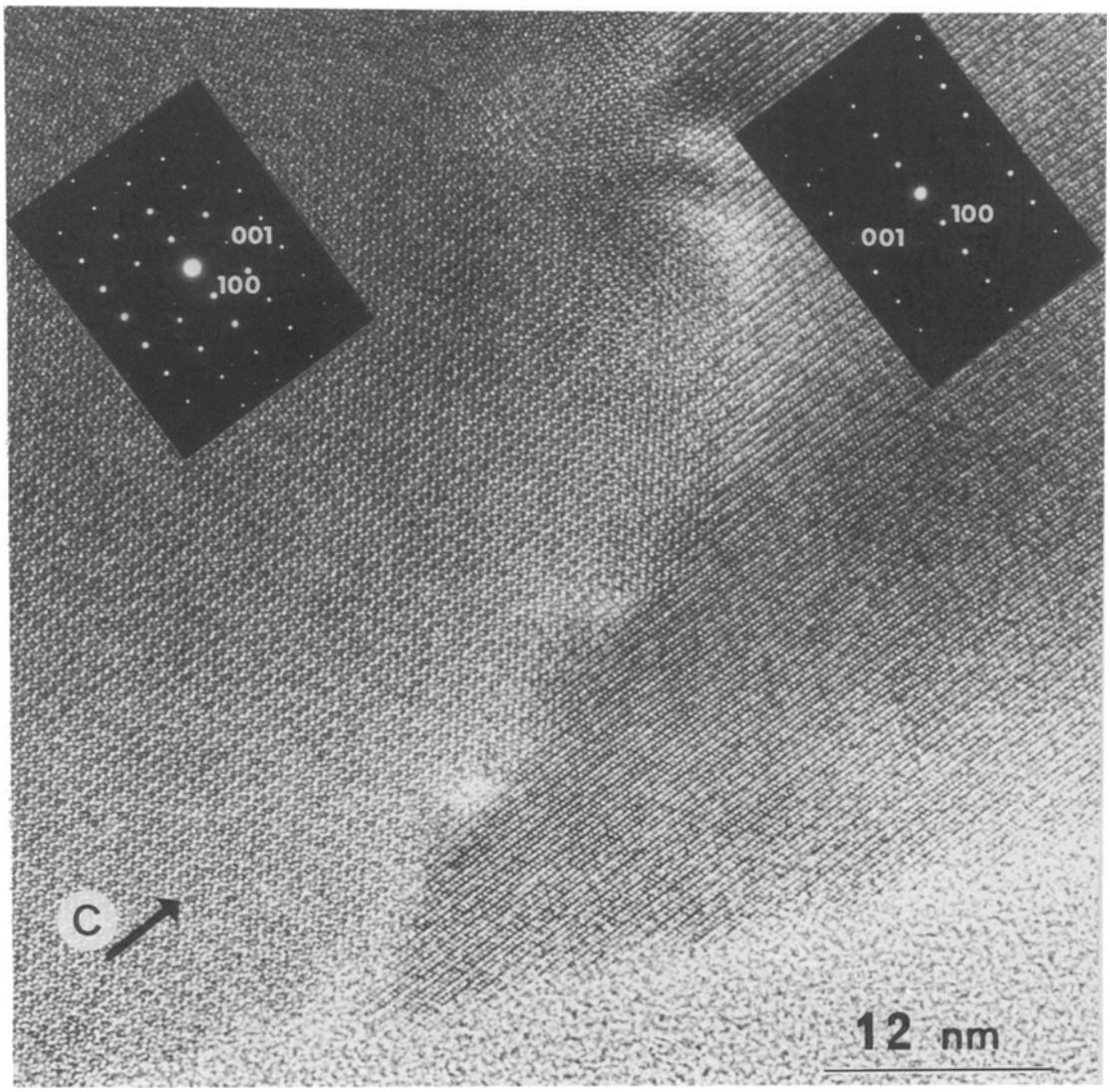

Figure 12 [1 0 0] image of coherent intergrowth of α- and β-sialon.

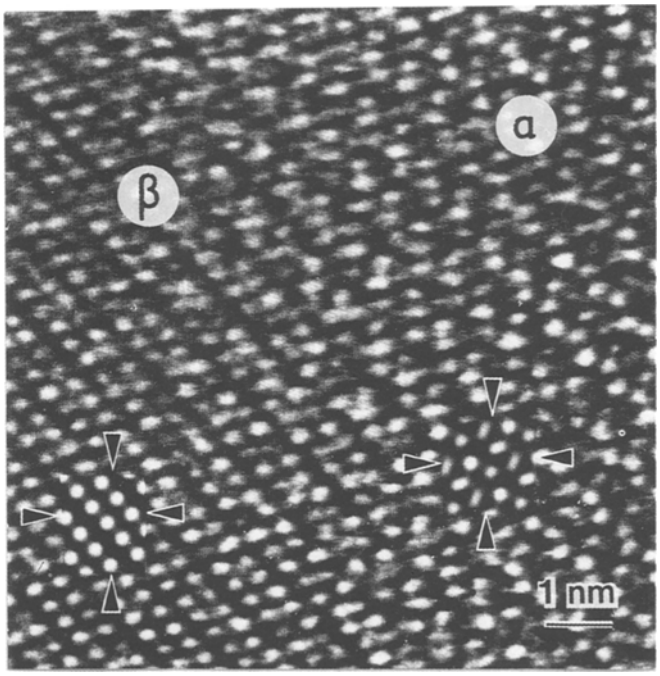

Figure 13 Calculated [1 0 0] images of α- and β-sialon inserted into an enlarged area of the crystal shown in Fig. 12. The simulated images (indicated by arrows) were calculated for a thickness of 12.0 nm and a defocus of −89.2 nm. The experimental image was transferred directly on-line to the image processing system.

defect (marked A in Fig. 5) there is an extra row of dots inserted in the lattice at right angles to the *c* axis. This gives an extra spacing of about half the *c* axis. Towards the edges of the defect it is seen how one of the rows gradually disappears. A plausible model for the part of the defect marked A is thus the insertion of an extra A–B layer into the normal sequence A–B–C–D along the *c* axis. In Fig. 6, a calculated image based on this model has been inserted in an enlarged part of the defect of Fig. 5.

Another type of fault orthogonal to the *c* axis in an α-sialon crystal is seen in Fig. 7. In contrast to the defects seen in Fig. 4 this fault extends throughout the whole crystal and involves shear of the lattice through a fraction of the projected *b* axis. The contrast on both sides changes along the defect with only a small part (enlarged in Fig. 7) having fairly equal contrast on both sides. It can be seen that the shift perpendicular to the *c* axis is approximately one third of the projection of the *a* axis. Indeed it is possible to make a translation of the unit cells $\frac{1}{3}a + \frac{2}{3}b$ and still keep the atomic distances and the bonding pattern across the defect approximately the same as in the normal structure (Fig. 8). Although this appears to be a plausible model, it has not been possible to obtain simulated images that match the observed image well. Apparently the detailed atomic arrangement is very critical and may vary along the fault, giving rise to variable contrast.

In addition to these intragranular defects, two cases of coherent intergrowth of α- and β-sialon have been observed. The first example is shown in Fig. 9. This image shows two areas (marked α and β) of the same crystal which are separated by a boundary consisting of alternating light and dark areas. No glassy phase can be detected along the border. A few planar faults of the type studied by Sasaki *et al.* [4] can be seen in the lower left part of the image. The two areas give rise to different diffraction pattens (seen in Fig. 10). By comparing these patterns with calculated ones, the zone axes could be determined to be $[\bar{1}\,2\,1]$ of α-sialon for one part and $[\bar{1}\,2\,2]$ of β-sialon for the other. This suggests that the *c* axis is a common direction for both parts. The crystal of Fig. 9 is seen at a larger magnification in Fig. 10. Here one can see that the contrast changes gradually from α to β across the boundary, which apparently is not parallel to the line of sight. In Fig. 11, calculated images for each phase have been inserted in a magnified part of Fig. 10. The two inserted images have been calculated for the same thickness and defocus.

A second example of α- and β-phase epitaxially grown together is shown in Fig. 12. The contrast is seen to change gradually from α to β within a transition zone. This is thus apparently also a boundary that is not parallel with the beam. In this case the two phases are viewed along the [1 0 0]- zone axis, with the projection containing the *c* axis. This shows, as suggested above, that indeed the *c* axis is a possible common direction for both phases. In Fig. 13 a magnified part of the same crystal is shown with two calculated images inserted, marked by arrows, for the α- and β- part of the crystal.

6. Discussion

The sialon crystals investigated have been found to incorporate a variety of defects. The different types of defects described in this paper have to our knowledge not been found in sialon materials other than the cerium-containing phase studied here. This could imply a special tendency for cerium to initiate defects in the lattice. This is then probably due to the different size of the atom in the two valence states. Ce^{4+} with an ionic radius Y^{3+} ($r = 0.093$ nm) in the α-sialon structure, while Ce^{3+} with an ionic radius of 0.111 nm seems to be slightly too large. It has been reported that Nd^{3+} ($r = 0.108$ nm) seems to be of about the maximum size for entering the voids of the α-structure [9, 13]. If this is so, only the tetravalent cerium would be able to stabilize the α-phase. Thus the inclusion of

the Ce^{3+}-ion in the lattice would probably initiate defects, especially if they are formed by reduction of Ce^{4+} at some stage of the annealing process.

The coherent intergrowth of α and β exemplifies two different phenomena; the existence of grain boundaries without intergranular phase and the transition from one phase to another within the same grain.

The question of the existence of an intergranular phase between grains in polyphase ceramic materials has been discussed in some detail by various authors [23–28]. An amorphous grain boundary layer with a thickness of about 1.5 to 2.0 nm between crystals was reported by Greil and Weiss [8]. This was confirmed by Clarke [26] who showed that from a thermodynamical point of view there should always exist some intergranular phase in polycrystalline ceramic materials. However, he also states that for special crystallographic directions, such as for example twin boundaries, coherent intergrowth could exist. In the present case there is obviously a distinct crystallographic relation between two phases which have a common plane including both c axes. This suggests that the change from one sialon phase to the other is accomplished by a change in stacking sequence from ABAB . . . to ABCD . . . corresponding to a 180° rotation of the CD layers (see above).

In an earlier article Clarke [25] gives three conditions which have to be fulfilled when using lattice imaging for detecting and determining the size of the intergranular glass phases in ceramic materials. These are: (1) the intergranular film must be observed edge-on if its true width is to be determined, (2) both adjacent grains should have favourable diffracting orientations and (3) the grains must be of a thickness at which the lattice fringes have high contrast. Since it was possible to calculate images such as those shown in Figs 11 and 13, the second and third conditions are obviously fulfilled. For the first condition in the present case, however, there is the possibility that the defect contrast seen across the borderline between the two different areas arises from two overlapping crystals. If there were an intergranular phase in between, the two lattices would hardly be in total register, and a moiré pattern would develop, which is, however, not seen. Instead, our results suggest that intergrowth with a common c axis is a possible way for the two different sialon phases to connect without any intergranular phase.

In addition to this, there is another feature of the image left to consider. When examining the transformation zone it is seen that well ordered areas alternate with less ordered parts (indicated with arrows in Fig. 10). The disordered areas are centred on edge dislocations. The presence of this kind of defect is due to the difference in length between the a axes of the two phases (α; $a = 0.7797$ nm, β; $a = 0.76203$ nm) and the fact that the c axis of the α-phase (0.5678 nm) is not exactly twice as long as the c axis of the β-phase (0.29190 nm). This has the consequence that the atomic planes which connect across the transformation zone are slightly differently spaced, ($d\alpha_{01\bar{2}} = 0.2617$ nm and $d\beta_{01\bar{1}} = 0.2669$ nm). This mismatch should give rise to an extra plane in the α crystal approximately every fiftieth plane, which is in fair agreement with observation. Due to the weaker atomic bonding in the less ordered parts, these areas are especially sensitive to grooving by the argon-ion beam, This means that the more diffuse contrast seen in these parts is plausible due either to a contamination layer or to the carbon coating filling the ion-beam-induced grooves [29].

The gradual change in contrast from the α-phase to the β-phase in the same crystal demonstrated in this study has not been reported before. The preparation method used, which makes such a transformation possible, involves a solid–liquid–solid mechanism, i.e., the starting material is dissolved in a liquid phase, and then the sialon-crystal is precipitated from the liquid. The crystal growth direction is preferably along the c axis [8]. Therefore a plausible explanation might be that during the growth of a β-sialon crystal the concentration of cerium and yttrium in the liquid surrounding the crystal is enhanced. At some point the concentration of cerium and yttrium has reached the value that stabilizes the α-sialon phase, which induces a 180° rotation of the CD layers. The reverse case is obviously also possible.

It can be noted that the defects reported in this paper have one crystallographic feature in common, namely the extension perpendicular to the c axis. As discussed above, a possible way to explain the occurrence of defects found in the material is that they are associated with changes in concentration which could act as defect initiations. Point analysis of intergranular phases has indeed shown that large compositional variations occur in this type of materials. The occurrence of local concentration differences is probably a result of the slow diffusion in these materials. The fact that in the present case CeO_2 with an ion of varying size and valency has been used as a sintering aid, could be another factor likely to initiate defects.

This sort of defect initiation due to the size of the stabilizing cation will be the subject of further studies. This includes various (Me, Me′)-sialon systems such as neodymium, lanthanum, cerium and yttrium.

Acknowledgements

The author wants to thank Professors Lars Kihlborg and Thommy Ekström and Mats Nygren for valuable discussions and comments on the manuscript. This investigation forms a part of a research project financed by the Swedish National Board for Technical Development.

References

1. K. HIRAGA, *Sci. Rep. Ritu, A-vol.* **32** (1984) 1.
2. K. M. KNOWLES, *Inst. Phys. Conf. Ser.* **78** (1985) 515.
3. H. KAKIBAYASHI, T. SHIMUTSO and F. NAGATA, *J. Electron. Microsc.* **34** (1985) 78.
4. K. SASAKI, K.KURODA, T. IMURA, H. SAKA and T. KAMINO, *J. Electron. Microsc.* **34** (1985) 414.
5. C. CHATFIELD, T. EKSTRÖM and M. MIKUS, *J. Mater. Sci.* **21** (1986) 2297.
6. M. MITOMO, Y. MORIYOSHI and J. SUZUKI, *J. Mater. Sci. Monogr.* (1983) 911.
7. H. SCHMID and M. RÜHLE, *J. Mater. Sci.* **19** (1984) 615.

8. P. GREIL and J. WEISS, *ibid* **17** (1982) 1571.
9. T. EKSTRÖM, M. NYGREN, P.-O. KÄLL and P.-O. OLSSON, *Mater. Sci. Eng.* **A105/106** (1988) 605.
10. I. C. HUSEBY and G. PETZOW, *Powder Metall. Int.* **6** (1974) 17.
11. F. F. LANGE, *Ceram. Bull.* **59** (1980) 239.
12. T. MAH, K. S. MAZDIYASNI and R. RUH, *Ceram. Bull.* **58** (1979) 840.
13. S. SLASOR, K. LIDELL and D. P. THOMPSON, *Special Ceramics* **8** (*British Ceramic Proc.* **37**) (1986) 51.
14. R. MARCHARD, Y. LAURENT and J. LANG, *Acta Crystallogr.* **B25** (1969) 2157.
15. R. GRÜN, *ibid.* **B35** (1979) 800.
16. F. IZUMI, M. MITOMO and Y. BANDO, *J. Mater. Sci.* **19** (1984) 3115.
17. F. K. VAN DIJEN, R. METSELAAR and R. B. HELMHOLDT, *J. Mater. Sci. Lett.* **6** (1987) 1101.
18. T. EKSTRÖM, M. NYGREN, P.-O. KÄLL and P.-O. OLSSON, *J. Mater. Sci.* **24** (1989) 1853.
19. M. A. O'KEEFE, (1984) in "Electron Optical Systems for Microscopy, Microanalysis and Microlithography", edited by J. J. Hren, F. A. Lenz, E. Munro, & P. B. Sewer, in Proceedings of the 3rd Pfeffercorn Conference, (SEM Inc., AMF O'Hara, IL 60666; USA).
20. G. R. GRINTON and J. M. COWLEY, *Optik* **34** (1971) 221.
21. S. IIJIMA, *Optik* **47** (1977) 438.
22. C. R. HUBBARD, H. E. SWANSON and F. A. MAUER, *J. Appl. Cryst.* **8** (1975) 45.
23. D. R. CLARKE, and G. THOMAS, *J. Amer. Ceram. Soc.* **60** (1977) 491.
24. L. K. VAN LOU, T. E. MITCHEL and A. H. HEUER, *J. Amer. Ceram. Soc.* **61** (1978) 392.
25. D. R. CLARKE, *Ultramic.* **4** (1979) 33.
26. *Idem., J. Amer. Ceram. Soc.* **70** (1987) 15.
27. C. B. CARTER, *in Proc. J. Mater. Res. Soc. Symp.* **31** (1984) 267.
28. C. B. CARTER and S. L. SASS, *J. Amer. Ceram. Soc.* **64** (1981) 335.
29. Y. KOUH SIMPSON, C. B. CARTER, K. J. MORRISSEY, P. ANGELINI and J. BENTLEY, *J. Mater. Sci.* **21** (1986) 2689.

Received 17 June
and accepted 7 December 1988